Journal of Geometry and Physics 62 (2012) 124–136

Contents lists available at SciVerse ScienceDirect

Journal of Geometry and Physics

journal homepage: www.elsevier.com/locate/jgp

Discrete spherical means of directional derivatives and Veronese maps

Alexander Belyaev [a], Boris Khesin [b], Serge Tabachnikov [c,*]

[a] Electrical, Electronic & Computer Engineering, Heriot–Watt University, Edinburgh, EH14 4AS, UK
[b] Department of Mathematics, University of Toronto, Toronto, ON M5S 2E4, Canada
[c] Department of Mathematics, Pennsylvania State University, University Park, PA 16801, USA

ARTICLE INFO

Article history:
Received 25 May 2011
Accepted 3 September 2011
Available online 29 September 2011

Keywords:
Finite differences
Discrete differential operators
Veronese maps
Minkowski theorem

ABSTRACT

We describe and study geometric properties of discrete circular and spherical means of directional derivatives of functions, as well as discrete approximations of higher order differential operators. For an arbitrary dimension, we present a general construction for obtaining discrete spherical means of directional derivatives. The construction is based on using Minkowski's existence theorem and Veronese maps. Approximating the directional derivatives by appropriate finite differences allows one to obtain finite difference operators with good rotation invariance properties. In particular, we use discrete circular and spherical means to derive discrete approximations of various linear and nonlinear first- and second-order differential operators, including discrete Laplacians. A practical potential of our approach is demonstrated by considering applications to nonlinear filtering of digital images and surface curvature estimation.

0. Introduction

Mean value properties of functions play a crucial role in the analysis of many partial differential equations [1], numerical interpolation and integration [2], computer tomography [3], and many other areas of mathematics and engineering. In this paper, we undertake a study of discrete circular and spherical means of directional derivatives of functions in view of their applications to the finite difference methods. We present a general construction for obtaining discrete spherical means of directional derivatives, analyze general properties of such means, and use them to derive finite difference approximations with good rotation-invariant properties for linear and nonlinear first- and second-order partial differential operators. The two principal components of our approach are based on the use of Minkowski's existence theorem [4] and Veronese maps [5].

For the sake of simplicity, we focus on finite difference approximations of very basic differential operators, the gradient and Laplacian. We start from an elementary analysis of discrete circular means of derivatives and demonstrate how such discrete means can be used for practical estimation of surface curvatures (Section 1). Then, in any dimension, we obtain Minkowski-type formulas for general and regular grids by using the Veronese map (Section 2). Finally, we analyze rotation invariance properties of discrete 2D gradient, Laplacian, and related nonlinear operators defined on a square grid (Section 3).

Various finite difference approximations of the gradient and Laplacian are widely used in fluid mechanics, electromagnetics, finance modeling, image processing, and many other areas. Our interest in constructing reliable discrete approximations of these operators is threefold. First, reliable and consistent approximations of the gradient and Laplacian are needed in various diffusion-type hydrodynamical models, such as the convection–diffusion equation

$$u_t + v \cdot \nabla u = \epsilon \Delta u,$$

* Corresponding author.
E-mail address: tabachni@math.psu.edu (S. Tabachnikov).

0393-0440/$ – see front matter
doi:10.1016/j.geomphys.2011.09.005

where the density u is convected by a velocity field v and dissipates at different time scales. Its attractors exhibit very peculiar behavior as $t \to \infty$ and $\epsilon \to 0$ (see [6]) and we hope that the approximation scheme developed in this paper could complement the analytic treatment of the attractors. The Laplacian case is also particularly useful in computations related to the fast dynamo problem, where the proposed approximation formulas may simplify computations of the magnetic diffusion for iterations of a seed magnetic field, see [7].

Secondly, linear and nonlinear diffusion-type equations are widely used in modern image processing for a variety of tasks including edge detection, image restoration, and image decomposition into structure and texture components [8, 9]. As demonstrated in [10], the use of discrete nonlinear diffusion operators with good rotation invariance properties is highly beneficial for such tasks. In addition, nonlinear image diffusion provides us with a useful testbed for the theoretical considerations below. Thirdly, accurate and reliable approximations of the surface gradient and Laplacian are key ingredients in many shape analysis studies. Below we discuss applications of the approximation formulas both in image processing and geometry. Finally we note that the approach via the Veronese map described in the present paper can also be used for higher order differential operators, such as bi-Laplacian.

1. Circular means of derivatives and their applications

Continuous and discrete circular means. A simple way to demonstrate the rotational invariance of the 2D Laplacian

$$\Delta \equiv \frac{\partial^2}{\partial x^2} + \frac{\partial^2}{\partial y^2}$$

consists of representing it as the circular mean (respectively, the spherical mean in 3D) of the second-order directional derivatives

$$\frac{1}{2}\Delta f = \frac{1}{\pi}\int_0^\pi \frac{\partial^2 f}{\partial \boldsymbol{e}_\varphi^2} d\varphi, \quad \text{where } \boldsymbol{e}_\varphi = (\cos\varphi, \sin\varphi)\,, \ \frac{\partial}{\partial \boldsymbol{e}_\varphi} = \cos\varphi\frac{\partial}{\partial x} + \sin\varphi\frac{\partial}{\partial y}. \tag{1}$$

The rotational invariance of the squared gradient $|\nabla f|^2$ can be demonstrated in a similar way as

$$\frac{1}{2}|\nabla f|^2 = \frac{1}{\pi}\int_0^\pi \left(\frac{\partial f}{\partial \boldsymbol{e}_\varphi}\right)^2 d\varphi. \tag{2}$$

More generally, the mean value representation for a directional derivative of f can be obtained from

$$\frac{1}{2}\left[a\frac{\partial f}{\partial x} + b\frac{\partial f}{\partial y}\right] = \frac{1}{\pi}\int_0^\pi [a\cos\varphi + b\sin\varphi]\,\frac{\partial f}{\partial \boldsymbol{e}_\varphi}\, d\varphi, \tag{3}$$

where a and b are constants. Notice that (3) with $a = \partial/\partial x$ and $b = \partial/\partial y$ implies (1) and setting $a = \partial f/\partial x$ and $b = \partial f/\partial y$ yields the equality (2).

Let us now derive discrete counterparts of the above mean value representations (1)–(3). Consider a set of directions $\boldsymbol{e}_k = (\cos\varphi_k, \sin\varphi_k)$, $k = 1, 2, \ldots, n$. Then a weighted sum of the second-order directional derivatives can be expressed as

$$\begin{aligned}\sum w_k \frac{\partial^2 f}{\partial \boldsymbol{e}_{\varphi_k}^2} &= \frac{\partial^2 f}{\partial x^2}\sum w_k \cos^2\varphi_k + \frac{\partial^2 f}{\partial y^2}\sum w_k \sin^2\varphi_k + 2\frac{\partial^2 f}{\partial x \partial y}\sum w_k \cos\varphi_k \sin\varphi_k = \frac{1}{2}\Delta f \sum w_k \\ &\quad + \frac{1}{2}\left(\frac{\partial^2 f}{\partial x^2} - \frac{\partial^2 f}{\partial y^2}\right)\mathrm{Re}\left(\sum w_k e^{2i\varphi_k}\right) + \frac{\partial^2 f}{\partial x \partial y}\mathrm{Im}\left(\sum w_k e^{2i\varphi_k}\right).\end{aligned} \tag{4}$$

Finding weights $\{w_k\}$ such that

$$\sum w_k e^{2i\varphi_k} = 0 \tag{5}$$

yields, after a simple normalization $\{w_k\} \longrightarrow \left\{w_k \Big/ \sum w_k\right\}$, a discrete mean value representation for Δf:

$$\frac{1}{2}\Delta f = \sum w_k \frac{\partial^2 f}{\partial \boldsymbol{e}_{\varphi_k}^2}, \tag{6}$$

and similar representations of the squared gradient

$$\frac{1}{2}|\nabla f|^2 = \sum w_k \left(\frac{\partial f}{\partial \boldsymbol{e}_{\varphi_k}}\right)^2 \tag{7}$$

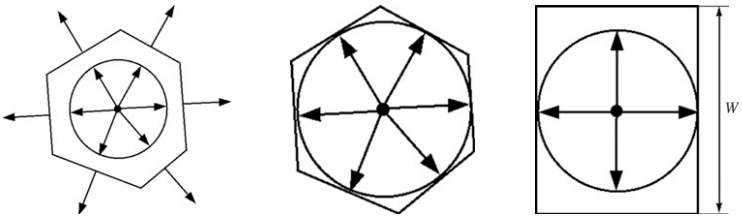

Fig. 1. Left: Minkowski's existence theorem for polygons provides us with a geometric interpretation of (5). Middle: a special case of a polygon circumscribed around the unit circle was considered in [11] in connection with the curvature estimation approach proposed there. Right: 3×3 stencils for estimating the gradient and Laplacian of functions defined on a square grid contain four directions and correspond to rectangles.

and directional derivative

$$\frac{1}{2}\left[a\frac{\partial f}{\partial x} + b\frac{\partial f}{\partial y}\right] = \sum w_k \left[a\cos\varphi_k + b\sin\varphi_k\right]\frac{\partial f}{\partial \boldsymbol{e}_{\varphi_k}}, \tag{8}$$

respectively. Obviously the same set of weights $\{w_k\}$ can be used to obtain a discrete mean value representation for a quasi-Laplacian

$$\frac{1}{2}\nabla\cdot(a(x,y)\nabla f) = \sum w_k \frac{\partial}{\partial \boldsymbol{e}_{\varphi_k}}\left(a(x,y)\frac{\partial f}{\partial \boldsymbol{e}_{\varphi_k}}\right). \tag{9}$$

Note that the appearance of double angles in the formula (5) exactly corresponds to the Veronese map $V : (\cos\phi, \sin\phi) \mapsto (\cos 2\phi, \sin 2\phi)$, considered in Example 2.4 of the next section.

Discrete mean value formulas and Minkowski's problem for polygons. The key problem of finding normalized weights $\{w_k \mid \sum w_k = 1\}$ in the relation $\sum w_k e^{2i\varphi_k} = 0$ (see (5) above) has a simple geometric meaning and is directly related to Minkowski's existence theorem (also called Minkowski's problem, see e.g. [4]) for polyhedra.

Theorem 1.1 (*Minkowski's Existence Theorem*)**.** *Consider unit vectors* $\mathbf{n}_1, \mathbf{n}_2, \ldots, \mathbf{n}_k$ *spanning* $\mathbf{R}^m$ *and a set of positive weights* $w_1, w_2, \ldots, w_k$*. Then the equation*

$$w_1\mathbf{n}_1 + w_2\mathbf{n}_2 + \cdots + w_k\mathbf{n}_k = 0$$

is a necessary and sufficient condition for existence of a convex polyhedron with facet unit normals $\mathbf{n}_1, \mathbf{n}_2, \ldots, \mathbf{n}_k$ *and corresponding facet areas* $w_1, w_2, \ldots, w_k$*. Further, this polyhedron is unique up to translation.*

The necessity part of this theorem is, of course, trivial and follows immediately from the Gauss divergence theorem.

Let us note that in (1)–(3) one deals with the directions $\boldsymbol{e}(\varphi) = (\cos\varphi, \sin\varphi)$, $0 \le \varphi < \pi$, which can be parameterized by the unit vector $e^{2i\varphi}$. Now consider a closed polygon such that the vectors $e^{2i\varphi_k}$ are the outward normals of the polygon's edges. Then, according to the Gauss divergence theorem, the edge lengths provide us with the desired set of weights $\{w_k\}$. Vice versa, given a set of unit vectors $\{e^{2i\varphi_k}\}$ and positive weights $\{w_k\}$ satisfying the first condition in (5), Minkowski's existence theorem guarantees an existence of a convex polygon with edge lengths $\{w_k\}$ and outward normals $e^{2i\varphi_k}$. The left image of Fig. 1 illustrates this geometric interpretation of (5).

In particular, if we consider a polygon circumscribed around the unit circle, as seen in the middle image of Fig. 1, the lengths of the polygon sides are given by

$$\tan\beta_{j-1} + \tan\beta_j, \qquad \beta_k = \varphi_{k+1} - \varphi_k,$$

and, therefore, the normalized weights are

$$w_j = \frac{\tan\beta_{j-1} + \tan\beta_j}{\sum(\tan\beta_{k-1} + \tan\beta_k)}. \tag{10}$$

This set of weights was used in [11] for estimating the mean curvature on surfaces approximated by dense triangle meshes.

In Section 2 we show how to solve this key problem in any dimension and, in particular, get a discretization of the corresponding Laplacian.

Application to curvature estimation. In the previous examples, we have considered function data defined on a regular grid. Here we deal with less organized data, namely with triangle meshes approximating smooth surfaces embedded into the Euclidean space $\mathbf{R}^3$.

Reliable estimation of curvature characteristics of polygonal surfaces is very important for many computer graphics and geometric modeling applications. Starting from a seminal paper of Taubin [12] integral-based approaches are frequently used for curvature estimation purposes [11,13,14] (see also references therein). Our approach to curvature estimation is based on using discrete circular means of directional surface derivatives. Given a smooth surface approximated by a dense triangle mesh, we employ such discrete circular means for estimating the mean curvature $H = (k_{\max} + k_{\min})/2$ and the

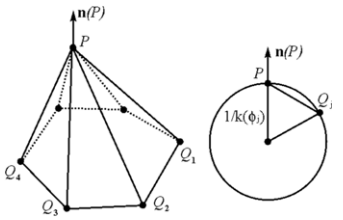

Fig. 2. Left: a mesh vertex P and its 1-ring neighboring vertices $\{Q_j\}$. Right: a geometric explanation of the directional curvature approximation in (14).

so-called curvedness [15] $R = \sqrt{\left(k_{\max}^2 + k_{\min}^2\right)/2}$, where $k_{\max}$ and $k_{\min}$ stand for the principal curvatures. (While the curvedness R is not a classical curvature measure, it is widely used in numerous applications including protein interaction analysis [16], heart physiology [17], and human visual perception [18].)

Let $\mathbf{n}$ be a surface orientation normal. Denote by $\mathbf{t}_{\max}$ and $\mathbf{t}_{\min}$ the principal directions corresponding to the principal curvatures $k_{\max}$ and $k_{\min}$, respectively. For a point P on the surface, consider a unit tangent vector $\mathbf{t}(\varphi)$, which makes angle φ with $\mathbf{t}_{\max}$, and the corresponding directional curvature $k(\varphi)$. Similar to (1) and (2) we have

$$H \equiv \frac{1}{2}\left(k_{\max} + k_{\min}\right) = \frac{1}{2\pi}\int_0^{2\pi} k(\varphi)\, d\varphi \tag{11}$$

and

$$R^2 \equiv \frac{1}{2}\left(k_{\max}^2 + k_{\min}^2\right) = \frac{1}{2\pi}\int_0^{2\pi} \left(\frac{\partial \mathbf{n}}{\partial \mathbf{t}(\varphi)}\right)^2 d\varphi, \tag{12}$$

respectively. Here (11) immediately follows from Euler's formula

$$k(\varphi) = k_{\max}\cos\varphi^2 + k_{\min}\sin\varphi^2$$

and (12) is obtained from a similar representation

$$\left(\frac{\partial \mathbf{n}}{\partial \mathbf{t}(\varphi)}\right)^2 = k_{\max}^2\cos^2\varphi + k_{\min}^2\sin^2\varphi,$$

which, in turn, can be easily derived from the Rodrigues formulas

$$\frac{\partial \mathbf{n}}{\partial \mathbf{t}_{\max}} = -k_{\max}\,\mathbf{t}_{\max}, \qquad \frac{\partial \mathbf{n}}{\partial \mathbf{t}_{\min}} = -k_{\min}\,\mathbf{t}_{\min}.$$

Similar to (6) and (7), let us consider discrete counterparts of (11) and (12)

$$H = \sum w_j k(\varphi_j) \quad \text{and} \quad R^2 = \sum w_j \left(\frac{\partial \mathbf{n}}{\partial \mathbf{t}(\varphi_j)}\right)^2, \tag{13}$$

where weights $\{w_j\}$ satisfy (5) and are normalized by $\sum w_k = 1$. For the sake of simplicity, we use the set of weights (10) proposed in [11].

Consider now a triangle mesh approximating the surface and assume that each mesh vertex P is equipped with a unit normal $\mathbf{n}(P)$ which delivers a fairly good approximation of the corresponding surface normal. Given a mesh vertex P and its 1-ring neighboring vertices $\{Q_j\}$, as seen in the left image of Fig. 2, simple approximations of tangential vectors at P and the corresponding directional curvature $k(\varphi_j)$ and directional derivative of $\mathbf{n}$ are given by

$$\mathbf{t}_j \approx \frac{\vec{PQ_j}}{\|P - Q_j\|}, \qquad k(\varphi_j) \approx \frac{2\vec{PQ_j}\cdot \mathbf{n}}{\|P - Q_j\|^2}, \qquad \frac{\partial \mathbf{n}}{\partial \mathbf{t}_j} \approx \frac{\mathbf{n}(Q_j) - \mathbf{n}(P)}{\|Q_j - P\|}, \tag{14}$$

respectively. We refer to the right image of Fig. 2 for a geometric explanation of the directional curvature approximation. Finally, (13) and (14) provide us with discrete approximations of the mean curvatures H and curvedness R.

Fig. 3 presents color encodings for the mean curvature H and curvedness R detected on a geometrical model with many small-scale details (see the electronic version of this paper for a color version of this figure).

A visual comparison of (13) and (14) with the curvature estimation methods developed in [12,13] indicates that our discretization is less robust to noise but better reflects small-scale surface details. One can improve the approximation by using more sophisticated approximations for the tangent directions, directional curvatures, and directional derivatives of the normal instead of common-sense estimates (14). Here our goal was to reveal potential applications of our approach to curvature-based shape analysis.

Fig. 3. Color encodings (please see the online version of this paper for this figure in color) for the mean curvature (left) and curvedness (right) detected on Gargoyle model (center).

2. Discrete spherical means of derivatives

General construction and Veronese maps. In this section we describe a generalization of the discrete mean value formulas of the preceding section from the circle case to arbitrary higher dimensions. In particular, we prove the following

Theorem 2.1. *Given a degree $k \neq 0$ and a collection of points P_i, $i = 1, \dots, N$, in general position on the unit sphere in $S^n \subset \mathbf{R}^{n+1}$, with $N > \binom{n+k-1}{n-1} - \binom{n+k-3}{n-1}$, there exist weights w_i (not all equal to zero) such that for every homogeneous polynomial F of the degree k one has $\sum_i w_i \cdot F(P_i) = 0$.*

For $k = 1$, we have $N > n$, and this theorem can be viewed as a direct corollary of Minkowski's theorem. Note that for a possible application to computations of the mean curvature of a manifold, the function F can be the sum of a constant ($k = 0$) and a homogeneous quadratic term ($k = 2$), and one needs to find the weights for obtaining the mean value $\bar{F}$ of such a function from its values at the given set of points. (Of course, all nonzero harmonics should give us the zero mean.) The cases of computations for the discrete Laplacian and square gradient operators are similar.

For instance, we use Theorem 2.1 to construct a discrete Laplacian as follows.

Definition 2.2. Let O be a vertex in an arbitrary irregular grid with neighboring vertices $\bar{P}_i$. Define the discrete Laplacian of a function f at a point O to be

$$\frac{1}{2}\Delta f(O) \coloneqq \sum w_i \frac{\partial^2 f}{\partial \boldsymbol{e}_{P_i}^2}, \tag{15}$$

where points P_i are normalized from $\bar{P}_i$ to lie on the unit sphere centered at O, the weights w_i are given by the above theorem for $k = 2$, and $\partial^2 f/\partial \boldsymbol{e}_{P_i}^2$ are discrete approximations of the second derivatives of f at O in the direction OP_i.

Definition (15) is inspired by formula (6) and, as we will see later, generalizes the standard discrete Laplacians defined on regular grids.

Remark 2.3. The result of Theorem 2.1 is very close to constructions of so called "spherical designs". The latter is a finite set of points on S^n such that the average value of any polynomial F of degree less than or equal to k on this set equals the average value of the polynomial F on the sphere. The concept of a spherical design was introduced in [19]. The existence and structure of spherical designs in a circle was studied in [20]. In [21] the existence of designs of all sufficiently large sizes was proved: there is a number $N(n, k)$ depending on n and k, such that a design exists for any $N > N(n, k)$. Many examples and recent results can be found in the survey [22].

The statement of Theorem 2.1 is somewhat different: we do not require the weights to be equal. In many applications, however, one uses the regular latices, and the weights turn out to be equal, as we discuss below.

Proof—Construction. First, we prove Theorem 2.1 for a linear functional L (i.e. for $k = 1$). In this case the solution is given by the Minkowski's Theorem 1.1. Namely, consider the tangent hyperplanes to the sphere S^n at points P_i; they form a polyhedron. (Here it suffices to assume that P_i, $i = 1, \dots, N$ are in general position, i.e., not lying at one hyperplane section of the sphere.) Let w_i be the signed codimension-one volumes of the faces of this polyhedron. Then $\sum_i w_i \cdot P_i = 0$ according to Minkowski's theorem (where we understand P_i as vectors in $\mathbf{R}^{n+1}$), and hence $\sum_i w_i \cdot L(P_i) = 0$ for every linear function.

Next, consider spherical harmonics of degree k, i.e. harmonic polynomials of degree k in $\mathbf{R}^{n+1}$ restricted to the sphere $S^n \subset \mathbf{R}^{n+1}$. One can confine to spherical harmonics for the proof of the general statement on all homogeneous degree k polynomials, since harmonic homogeneous polynomials give exactly all independent restrictions of homogeneous polynomials of degree k from $\mathbf{R}^{n+1}$ to the sphere. (We will need the restrictions of $x_1^2, \dots, x_{n+1}^2$ for the curvature function.)

Now we consider the harmonic Veronese map $V : \mathbf{R}^{n+1} \to \mathbf{R}^q$, where $V(x_1, \dots, x_{n+1}) = (x_1^k - x_2^k, \dots)$, that is, the map defined by taking a basis of harmonic polynomials in $x_1, \dots, x_{n+1}$ of degree k. The dimension q is given by the formula: $q = \binom{n+k-1}{n-1} - \binom{n+k-3}{n-1}$. Then $F = L \circ V$ where L is a linear function on $\mathbf{R}^q$. Let w_j be the constructed above weights for the collection of points $V(P_j)$ in $\mathbf{R}^q$. This gives us the required formula $\sum_i w_i \cdot F(P_i) = 0$.

Example 2.4. Let us demonstrate this approach in the case of a circle S^1 and quadratic functions. The harmonic Veronese map for quadratic polynomials sends the coordinate functions $\{x_1, \ldots, x_{n+1}\}$ to the space of quadratic harmonic polynomials (whose restrictions on the sphere S^n give us spherical harmonics). For the circle $S^1 \subset \mathbf{R}^2$ this harmonic Veronese map is $V : \mathbf{R}^2 \to \mathbf{R}^2$, where $(x, y) \mapsto (x^2 - y^2, 2xy)$, or $(\cos\phi, \sin\phi) \mapsto (\cos 2\phi, \sin 2\phi)$, see a detailed analysis in the preceding section.

Note that if we map $\mathbf{R}^2_{x,y}$ to the full 3-dimensional space $\mathbf{R}^3$ of quadratic polynomials $(x^2, y^2, 2xy)$, then the image of the circle $S^1 \subset \mathbf{R}^2$ will lie in the plane $\mathbf{R}^2 \subset \mathbf{R}^3$ (due to the relation $x^2 + y^2 = 1$), so the point images $V(P_i)$ will not be in general position to yield a polyhedron circumscribed around a 2-sphere in $\mathbf{R}^3$.

Example 2.5. For the case of 2-sphere and quadratic functions the space of harmonic polynomials is 5-dimensional, and our harmonic Veronese map sends S^2 to this $\mathbf{R}^5$. The point images lie in general position, and sufficiently many points (at least 6) would yield a polyhedron, which allows one to find the corresponding weights w_i.

Remark 2.6. Since the points $Q_j = V(P_j)$ should lie on the sphere S^{q-1}, rather than be generic vectors in $\mathbf{R}^q$, one can project them to the sphere by rescaling. Namely, let Q_j be a (sufficiently generic) collection of non-zero vectors in $\mathbf{R}^q$. Assign the following weights w_j to these vectors. Consider the collection of points $Q_j/|Q_j|$ on the unit sphere S^{q-1}, draw the tangent hyperplanes to the sphere, and let u_j be the signed $(q-1)$-dimensional volumes of the faces of the resulting polyhedron.

Proposition 2.7. *For every linear function L on $\mathbf{R}^q$, one has: $\sum_j w_j \cdot L(Q_j) = 0$, where the weights are $w_j := u_j/|Q_j|$.*

Proof. Minkowski's formula says that $\sum u_j \cdot Q_j/|Q_j| = 0$, hence $0 = \sum u_j \cdot L(Q_j)/|Q_j| = \sum_j w_j \cdot L(Q_j)$. □

Weights for regular lattices. Now, from the general consideration of points in general position we move to regular ones, and consider the set of all "m-mid-points", i.e., the set $M_m \subset S^n$ of points whose coordinates are all possible combinations of m nonzero coordinates equal to ± 1 among n spots, starting with $(\pm 1, \ldots, \pm 1, 0, \ldots, 0)$ to $(0, \ldots, 0, \pm 1, \ldots, \pm 1)$, which are scaled to belong to the unit sphere $S^n \subset \mathbf{R}^{n+1}$. Here m is any fixed integer between 1 and n. We also confine to the case of quadratic harmonics, $k = 2$ in the general problem above.

Example 2.8. In dimension 3, for $m = 1$ we get M_1 consisting of 6 midpoints of the cube faces, which are also the vertices of an octahedron: $(\pm 1, 0, 0)$, $(0, \pm 1, 0)$ and $(0, 0, \pm 1)$. The set M_2 consists of 12 scaled mid-points of the cube edges: $(\pm 1, \pm 1, 0)/\sqrt{2}$, $(\pm 1, 0, \pm 1)/\sqrt{2}$, and $(0, \pm 1, \pm 1)/\sqrt{2}$. The set M_3 contains exactly 8 vertices of the cube: $(\pm 1, \pm 1, \pm 1)/\sqrt{3}$.

Theorem 2.9. *Let $F(x_1, \ldots, x_{n+1})$ be a homogeneous quadratic function, $M_m \subset S^n$ be the set of m-mid-points for any fixed m, $1 \le m \le n$. Then*

$$\frac{1}{\mathrm{vol}(S^n)} \int_{S^n} F dS = \frac{1}{\#M_m} \sum_{x \in M_m} F(x),$$

where $\mathrm{vol}(S^n)$ is the volume of n-dimensional sphere and $\#M_m$ is the number of points in M_m.

One can see that in all these "regular cases" one counts the points of M_m with equal weights. This theorem generalizes the corresponding 3D consideration (see e.g. [23]), which gives three basis stencils used in the Laplacian computations.

Proof. Write $F = c + G$, where $c \in \mathbf{R}$ and G a harmonic quadratic polynomial. For a constant c the claim is obvious. For G one has $\int_{S^n} G dS = 0$, so we need to show that $\sum_{x \in M_m} G(x) = 0$ for every harmonic quadratic polynomial G.

Consider the full Veronese map $\overline{V} : \mathbf{R}^n \to \mathbf{R}^{q+1}$, given by

$$(x_1, \ldots, x_{n+1}) \mapsto (x_1^2, \ldots, x_{n+1}^2; x_1x_2, \ldots, x_nx_{n+1}),$$

with $q + 1 = (n + 1)(n + 2)/2$. Let $\mathcal{H}$ be the space of linear functions on $\mathbf{R}^{q+1}$ that vanish on the vector $\xi = (1, \ldots, 1; 0, \ldots, 0)$ with first $n + 1$ nonzero components (we separate them by semicolon). Then, for each quadratic harmonic G, one has $G = H \circ \overline{V}$ for some $H \in \mathcal{H}$. Indeed, harmonic polynomials form a hyperplane in the space of linear functions on $\mathbf{R}^{q+1}$ being given by one linear relation (coming from the sphere equation $x_1^2 + \cdots + x_{n+1}^2 = 1$), and the polynomials $x_1^2 - x_2^2, \ldots, x_n^2 - x_{n+1}^2, x_1x_2, \ldots, x_nx_{n+1}$ are harmonic and equal to 0 on this vector ξ. Thus we need to check that $\sum_{Q \in \overline{V}(M_m)} H(Q) = 0$ for all $H \in \mathcal{H}$ and any $m = 1, \ldots, n + 1$.

For instance, for the set M_1, which consists of $(0, \ldots, 0, \pm 1, 0, \ldots, 0)$-type points, the image $\overline{V}(M_1)$ consists of vectors Q_i: $(0, \ldots, 0, 1, 0, \ldots, 0; 0, \ldots 0)$ with 1's in one of the first n coordinates. In the case of M_2 with $2n(n - 1)$ "diagonal" points

$$(0, \ldots, 0, \pm 1, 0, \ldots, 0, \pm 1, 0, \ldots, 0)/\sqrt{2},$$

the image $\overline{V}(M_2)$ consists of vectors Q_i:

$$(0, \ldots, 0, 1, 0, \ldots, 0, 1, 0, \ldots, 0; 0, \ldots, 0, \pm 1, 0, \ldots, 0)/2$$

with all possible pairs of 1's among first $n+1$ coordinates and the ± 1 at the respective, ij-place. Similarly, for any m one can see that in each of these cases we have $\sum_1^{\#M_m} Q_i = const \cdot \xi$. Hence $\sum_1^{\#M_m} H(Q_i) = 0$ for all $H \in \mathcal{H}$, as claimed. □

Thus, while Theorem 2.1 allows one to find the weights w_i for a generic set of vectors P_i, Theorem 2.9 gives the explicit weights in the case when F is a homogeneous quadratic polynomial (i.e., $k = 2$) and vectors P_i correspond to the m-mid-points of the n-dimensional cube, $1 \le m \le n$.

Remark 2.10. For computations we are often interested mostly in the case $S^2 \subset \mathbf{R}^3$. Here is the explicit statement for $M = M_2$ adjusted to this case: let $F(x, y, z)$ be a homogeneous quadratic function, $M \subset S^2$ be the set of 12 points: $(\pm 1, \pm 1, 0)/\sqrt{2}$, $(\pm 1, 0, \pm 1)/\sqrt{2}$, and $(0, \pm 1, \pm 1)/\sqrt{2}$. Then

$$\frac{1}{4\pi} \int_{S^2} F dS = \frac{1}{12} \sum_{P \in M} F(P).$$

Thus in all of the above cases we need to use the same weights on these points. This equality of weights for a given set M_m can also be obtained from the symmetry consideration. One can also take combination of the above lattices M_m with *any weights* (provided that the sum of the weights is equal to 1), e.g., by considering arbitrary combinations of the 3 lattices in $\mathbf{R}^3$: mid-edges, vertices of the cube, and at the middle of faces. By imposing additional requirements, one can optimize these coefficients: for instance, to achieve an isotropic approximation, or with the next approximation smallest in an appropriate sense.

Remark 2.11. Points of $\overline{V}(M_1)$, evidently, form the coordinate $(n+1)$-simplex in the space spanned by first $n+1$ coordinates, which is a slim subspace in $\mathbf{R}^{q+1}$. In the case of M_2, the points of $\overline{V}(M_2)$ form the standard q-simplex in a hyperplane in $\mathbf{R}^{q+1}$. Indeed, in the latter case, we see that for all $Q_i \in \overline{V}(M_2)$ one has $(Q_i, Q_j) = 1/2$ for $i \ne j$ and $(Q_i, Q_i) = 3/4$, i.e., the vectors Q_i have the same length and same angles between them.

Remark 2.12. Above we considered two discretization procedures, both using the Veronese map: a generic set of points $\{P_i\}$ and the mid-points sets. While for a generic set in $\mathbf{R}^{q+1}$ the coefficients are given by Minkowski's formula for the corresponding polyhedron in the image, it is not the case in the mid-point cases. Indeed, due to a very regular structure of the image points $Q_j = \overline{V}(P_j)$, the corresponding tangent planes go to infinity, and the corresponding volumes of the faces are infinite.

In a sense, if the image points Q_j are linearly dependent in $\mathbf{R}^{q+1}$ (mod ξ), and the corresponding polyhedron has faces going to infinity (like in the standard basis case), we have to quotient out these "directions to infinity", and consider the volume of faces in a polyhedron of smaller dimension.

Example 2.13. For $n = 2$ and for the standard basis we did not get a polygon on the plane $\mathbf{R}^2 = \mathbf{R}^3$ (mod ξ). Instead, it reduces to a pair of points in $\mathbf{R}^1$. It is not enough to start with two generic points in this case, but if we take three generic points on the circle, we obtain an interpolation formula. This is a manifestation of the general phenomenon described in the following proposition.

Proposition 2.14. *There is no discrete mean value formula for quadratic harmonics and a given generic collection of $n+1$ points on S^n.*

Proof. Let $P_1, \ldots, P_{n+1} \in S^n$, and let $\overline{V} : \mathbf{R}^{n+1} \to \mathbf{R}^{q+1}$ with $q+1 = (n+1)(n+2)/2$ be the full Veronese map:

$$(x_1, \ldots, x_n) \mapsto (x_1^2, \ldots, x_{n+1}^2; x_1x_2, \ldots, x_ix_j, \ldots).$$

Let $\overline{V}(P_k) = Q_k$. Let $\xi = (1, \ldots, 1; 0, \ldots, 0) \in \mathbf{R}^{q+1}$.

We want to find constants w_k such that $\sum w_k \cdot Q_k = \xi$. This is equivalent to the following equality:

$$\mathrm{Diag}(w_k) = (A^*A)^{-1},$$

where A is the matrix made of the vectors $P_1, \ldots, P_{n+1}$, as the following linear algebra shows. Indeed, the equality $\sum w_kQ_k = \xi$ is equivalent to

$$\sum_i w_i x_{k,i} x_{l,i} = \delta_{k,l},$$

which is equivalent to $A \cdot \mathrm{Diag}(w) \cdot A^* = E$, the identity matrix. This is equivalent to $(A^*A)^{-1} = \mathrm{Diag}(w)$, as claimed.

Of course, if $\{P_k\}$ is an orthonormal frame then A is orthogonal, and all $w_k = 1$, as in the theorem above. The matrix AA^* is diagonal if and only if the vectors P_i are pairwise orthogonal. This is the case for the set M_1 discussed above, which consists of the basis points, but, of course, not true for generic collection of $n+1$ points on S^n. This implies that one cannot have an interpolation formula with $n+1$ generic points. □

Note that on the other hand, if one has sufficiently many points, so that their Veronese images are linearly dependent in $\mathbf{R}^{n(n+1)/2} \pmod{\xi}$, then any such linear relation provides the weights that yield an interpolation formula.

Higher-dimensional Laplacian approximation formulas. The results of the present section allow one to easily construct various discrete Laplacians and squared gradient similar to representations (6) and (7), respectively. In the beginning of the section we discussed the construction of the discrete Laplacian for an arbitrary grid, see formula (15):

$$\frac{1}{2}\Delta f(O) = \sum w_i \frac{\partial^2 f}{\partial \boldsymbol{e}_{P_i}^2}.$$

To obtain the weights w_i for a point O with neighboring vertices $\bar{P}_i$ we first normalize the latter to get P_i lying on the unit sphere centered at O. Then we consider the Veronese map and obtain points Q_i. Finally we obtain the weights $w_i = u_i/|Q_i|$ by finding the signed $(q-1)$-dimensional volumes u_i of the faces of the polyhedron in the Q-space, see Proposition 2.7. An analogue of the formula (7) for the square gradient instead of the Laplacian is completely analogous.

For a regular grid, Theorem 2.9 delivers similar formulas for a discrete Laplace operator where all weights w_i are equal:

$$\Delta f(O) = C_m \sum \frac{\partial^2 f}{\partial \boldsymbol{e}_{P_i}^2}, \tag{16}$$

where points P_i belong to the grid of m-midpoints, $P_i \in M_m$, and the constant C_m normalizes the sum, $C_m = \#M_1/\#M_m$, by comparing the number of neighbors in M_m with that in the coordinate grid M_1, the most straightforward definition of the discrete Laplacian.

Furthermore, one can consider linear combination of the Laplace approximations (16) with different coefficients α_m satisfying $\sum_{m=1}^{n} \alpha_m = 1$. Any such linear combination delivers a different discrete Laplacian and one can run a separate optimization problem on these coefficients α_m to find a discrete Laplacian with better rotation-invariant properties. We discuss the work in this direction for the 2D Laplacian in the next section.

3. Discrete circular means of derivatives and isotropic finite differences

In this section we show how to use discrete circular means of Section 1 for approximation of various differential operators in 2D by finite differences with good rotation invariance properties.

The simplest way to construct such approximations consists of substituting in (6)–(9) three-point finite differences instead of the first- and second-order derivatives. For example, constructing a discrete Laplacian corresponding to (6) can be done as follows. Consider a point $\mathbf{p}$ inside a convex bounded domain Ω. Let the straight line determined by $\mathbf{p}$ and direction $\boldsymbol{e}_\varphi$ intersect the boundary $\partial\Omega$ in two points $\mathbf{q}_1$ and $\mathbf{q}_2$. Denote by ρ_1 and ρ_2 the distances from $\mathbf{p}$ to $\mathbf{q}_1$ and $\mathbf{q}_2$, respectively. The second-order $\boldsymbol{e}_\varphi$-directional derivative of $f(\mathbf{p})$ can be approximated by

$$\frac{\partial^2 f}{\partial \boldsymbol{e}_\varphi^2} \approx \frac{2}{\rho_1\rho_2}\left(\left[\frac{f(\mathbf{q}_1)}{\rho_1} + \frac{f(\mathbf{q}_2)}{\rho_2}\right] \Big/ \left[\frac{1}{\rho_1} + \frac{1}{\rho_2}\right] - f(\mathbf{p})\right), \tag{17}$$

where ρ_1 and ρ_2 are assumed to be small. Now a discrete approximation of the Laplacian is obtained by summing up (17) over the set of directions $\boldsymbol{e}_{\varphi_k}$, $k = 1, 2, \ldots, n$.

Discrete Laplacian (6), (17) can be considered as a special case of a general construction studied in [24] (see also references therein).

It is interesting to note that integration of (17) with respect to φ

$$\Delta f(\mathbf{p}) \approx \int_0^{2\pi} \left[\left(\frac{f(\mathbf{q}_1)}{\rho_1} + \frac{f(\mathbf{q}_2)}{\rho_2}\right) \Big/ \left(\frac{1}{\rho_1} + \frac{1}{\rho_2}\right)\right] \frac{d\varphi}{\rho_1\rho_2} \Big/ \int_0^{2\pi} \frac{d\varphi}{\rho_1\rho_2} - f(\mathbf{p}) \tag{18}$$

leads to an extension of a pseudo-harmonic interpolation scheme proposed in [25]. It can be shown that, given $f(\mathbf{q})$ defined on $\partial\Omega$, (18) and its generalizations deliver the harmonic interpolation if Ω is a circle (a ball in the multidimensional case) [26].

Unfortunately combining circular means with directional finite differences does not automatically guarantee rotation invariance properties of the approximating differential operators. The reason is that the finite differences introduce directional errors. However, as seen below, for a regular grid, such directional errors can be uniformly distributed over the directions by choosing appropriate weights in discrete circular means (6)–(9).

Gradient and Laplacian stencils for square grids. Now let us focus on analyzing rotation invariance properties of regular grid stencils corresponding to (6) and (7).

Consider a two-dimensional square grid with step-size $h \ll 1$. Each grid vertex has eight nearest neighbors: two horizontal, two vertical, and four diagonal. Thus, according to our geometric interpretation of (6)–(8), we are given four directions and corresponding unit normals

$$\left\{e^{2i\varphi}\right\}, \quad \varphi = 0, \pi/4, \pi/2, 3\pi/4$$

which define a rectangle aligned with the coordinate axes.

Consider such a rectangle with the edge lengths 2 and w, as shown in the right image of Fig. 1, and replace the first- and second-order directional derivatives in (6)–(8) by corresponding central differences. We arrive at the following stencils for the x-derivative and Laplacian

$$\frac{\partial}{\partial x} \approx D_x \equiv \frac{1}{2h(w+2)} \begin{bmatrix} -1 & 0 & 1 \\ -w & 0 & w \\ -1 & 0 & 1 \end{bmatrix} \tag{19}$$

and

$$\Delta \approx L_\Delta \equiv \frac{1}{h^2(w+2)} \begin{bmatrix} 1 & w & 1 \\ w & -4(w+1) & w \\ 1 & w & 1 \end{bmatrix}, \tag{20}$$

respectively. The stencil D_y for $\partial/\partial y$ is obtained from D_x by $\pi/2$-rotation. Here and everywhere below the 3×3 matrices are understood as finite difference operators acting on functions defined on a square grid with step-size h.

Formulas (19) and (20) provide us with consistent parameterizations of the 3×3 stencils for the gradient and Laplacian.

Remark 3.1. The standard central difference and five-point Laplacian L_+ is obtained for $w = \infty$. Setting $w = 1$ leads to the so-called Prewitt masks for the 1st-order derivatives and Laplacian [27,28]. The case $w = 2$ is commonly used in image processing applications and yields the standard Sobel mask for the derivative [27,28] and a 9-point discrete Laplacian, which possesses good isotropic properties [29]. The case $w = 4$ was analyzed in [30], where it was shown that

$$D_x|_{w=4} = \frac{1}{8h} \begin{bmatrix} -1 & 0 & 1 \\ -4 & 0 & 4 \\ -1 & 0 & 1 \end{bmatrix} = \frac{\partial}{\partial x} + \frac{h^2}{12} \Delta \frac{\partial}{\partial x} + O(h^4), \tag{21}$$

$$L_\Delta|_{w=4} = \frac{1}{6h^2} \begin{bmatrix} 1 & 4 & 1 \\ 4 & -20 & 4 \\ 1 & 4 & 1 \end{bmatrix} = \Delta + \frac{h^2}{12} \Delta^2 + O(h^4), \tag{22}$$

as $h \to 0$. Since the Laplacian is isotropic, the right hand sides of (21) and (22) deliver asymptotically optimal asymptotically rotation-equivariant 3×3 stencils for the x-derivative and Laplacian, respectively, as $h \ll 1$. In particular, this explains why (20) with $w = 4$ is often used for a numerical solution of the Poisson equation [31, Chapter 3, Section 1], [32, Chapter 3, Section 10].

Discrete nine-point Laplacian (20) can be represented as a linear combination of two basis five-point Laplacians

$$L_\Delta = \alpha L_+ + \beta L_\times \quad \text{with } \alpha = \frac{w}{w+2} \text{ and } \beta = \frac{2}{w+2}, \text{ where}$$

$$L_+ = \frac{1}{h^2} \begin{bmatrix} 0 & 1 & 0 \\ 1 & -4 & 1 \\ 0 & 1 & 0 \end{bmatrix} \quad \text{and} \quad L_\times = \frac{1}{2h^2} \begin{bmatrix} 1 & 0 & 1 \\ 0 & -4 & 0 \\ 1 & 0 & 1 \end{bmatrix}.$$

Setting $w = 4$ yields $\alpha = 2/3$ and $\beta = 1/3$.

In Fig. 4, we use a Gaussian bump function

$$g(x, y) = \exp\left(x^2 + y^2\right) \tag{23}$$

to test isotropic properties of four discrete stencils

$$L_\Delta|_{w=\infty} \equiv L_+, \qquad L_\Delta|_{w=0} \equiv L_\times, \qquad L_\Delta|_{w=2}, \quad \text{and} \quad L_\Delta|_{w=4}.$$

Namely, the figure displays contour lines of $(\Delta - L_\Delta)[g]$. As (22) suggests, L_Δ with $w = 4$ demonstrates the best performance if the grid step-size h is sufficiently small.

Similar results are obtained for the x-derivative 3×3 stencils (19) and corresponding y-derivative stencil. Analogously to the case of the Laplacian, expansion (21) implies that (19) with $w = 4$ is rotationally optimal for sufficiently small h.

Remark 3.2. It is easy to increase the approximation accuracy of (21) and (22). For example, one can rewrite (21) as

$$\frac{\partial}{\partial x} = \left(1 + \frac{1}{h^2}\Delta\right)^{-1} D_x|_{w=4} + O(h^4) = \left(1 - \frac{1}{h^2}\Delta\right) D_x|_{w=4} + O(h^4)$$

and use stencil (22) for approximating Δ.

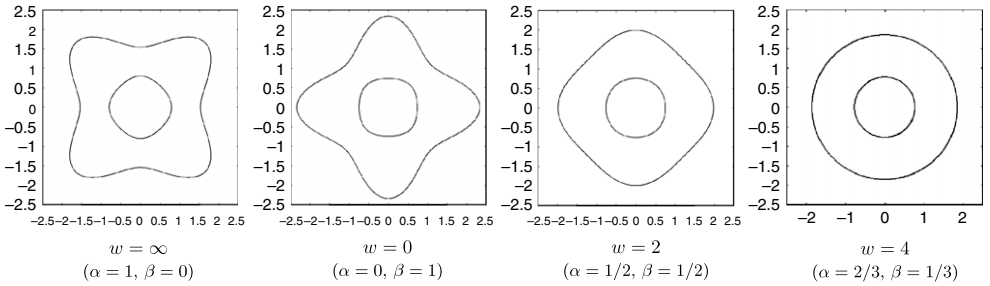

Fig. 4. Contour lines of $(\Delta - L_\Delta)[g]$ for various values of w. The best performance is achieved for $w = 4$.

Quasi-Laplacian stencil with good rotation invariance properties. Consider now a quasi-Laplacian operator

$$L^a \equiv \nabla \cdot [a(x, y)\nabla] = a\Delta + \nabla a \cdot \nabla \tag{24}$$

where $a(x, y)$ is given. In view of (22), (21) and (9), the optimal 3×3 stencils for L^a are obtained from (20) and (19) when $w = 4$.

In practice, the diffusion coefficient $a(x, y)$ in (24) is defined at the staggered grid points which lie on halfway between the standard grid points. Following [9, A.3.2] let us approximate (24) using a linear combination of two basis stencils

$$\alpha L^a_+ + \beta L^a_\times$$

with

$$L^a_+[f] \equiv \frac{1}{h^2}\left[a_{+0}f_{i+1,j} + a_{-0}f_{i-1,j} + a_{0+}f_{i,j+1} + a_{0-}f_{i,j-1} - (a_{+0} + a_{-0} + a_{0+} + a_{0-})f_{i,j}\right]$$

and

$$L^a_\times[f] \equiv \frac{1}{2h^2}\left[a_{++}f_{i+1,j+1} + a_{--}f_{i-1,j+1} + a_{+-}f_{i+1,j-1} + a_{--}f_{i-1,j-1} - (a_{++} + a_{-+} + a_{+-} + a_{--})f_{i,j}\right],$$

where $a_{\pm 0}$, $a_{0\pm}$, and $a_{\pm\pm}$ denote the values of $a(x, y)$ at $((i \pm 1/2)h, jh)$, $(ih, (j \pm 1/2)h)$, and $((i \pm 1/2)h, (j \pm 1/2)h)$, respectively.

Assume $h \ll 1$. Since the same weights are used in the discrete directional mean value representations (6) and (9) we can expect that the optimal rotation-invariant stencil for quasi-Laplacian L^a is obtained when $\alpha = 2/3$ and $\beta = 1/3$, or equivalently, when $w = 4$. This indeed turns out to be the case in the lower order terms:

Proposition 3.3. *The discrete approximation $\alpha L^a_+ + \beta L^a_\times$ of the quasi-Laplacian L^a is asymptotically rotation-equivariant for $\alpha = 2/3$ and $\beta = 1/3$ up to order $O\left(h^3\right)$ as $h \to 0$.*

Proof. A straightforward calculation shows that

$$L^a[f] = \nabla \cdot [a(x, y)\nabla f] + \frac{h^2}{12}\left[D_{0,4}(a, f) + 2D_{1,3}(a, f) + \frac{3}{2}D_{2,2}(a, f) + \frac{1}{2}D_{3,1}(a, f)\right] + O\left(h^4\right) \tag{25}$$

with

$$D_{0,4}(a, f) = a(x, y)\left(\frac{\partial^4 f}{\partial x^4} + 2\frac{\partial^4 f}{\partial x^2 \partial y^2} + \frac{\partial^4 f}{\partial y^4}\right),$$

$$D_{1,3}(a, f) = \frac{\partial a}{\partial x}\frac{\partial^3 f}{\partial x^3} + \frac{\partial a}{\partial y}\frac{\partial^3 f}{\partial x^2 \partial y} + \frac{\partial a}{\partial x}\frac{\partial^3 f}{\partial x \partial y^2} + \frac{\partial a}{\partial y}\frac{\partial^3 f}{\partial y^3},$$

$$D_{2,2}(a, f) = \frac{\partial^2 a}{\partial x^2}\frac{\partial^2 f}{\partial x^2} + \frac{\partial^2 a}{\partial y^2}\frac{\partial^2 f}{\partial y^2} + \frac{4}{3}\frac{\partial^2 a}{\partial x \partial y}\frac{\partial^2 f}{\partial x \partial y} + \frac{1}{3}\frac{\partial^2 a}{\partial x^2}\frac{\partial^2 f}{\partial y^2} + \frac{1}{3}\frac{\partial^2 a}{\partial y^2}\frac{\partial^2 f}{\partial x^2},$$

$$D_{3,1}(a, f) = \frac{\partial^3 a}{\partial x^3}\frac{\partial f}{\partial x} + \frac{\partial^3 a}{\partial x^2 \partial y}\frac{\partial f}{\partial y} + \frac{\partial^3 a}{\partial x \partial y^2}\frac{\partial f}{\partial x} + \frac{\partial^3 a}{\partial y^3}\frac{\partial f}{\partial y}.$$

It is interesting that expansion (25) does not contain h^3-terms.

Let us now demonstrate that these differential quantities are rotationally invariant. Obviously $D_{0,4}(a, f)$ equals $a(x, y)\Delta^2 f$ which is rotationally invariant. Let us consider

$$R_{1,3}(a, f, \varphi) = \frac{\partial a}{\partial e_\varphi} \cdot \frac{\partial^3 f}{\partial e^3_\varphi}, \qquad R_{2,2}(a, f, \varphi) = \frac{\partial^2 a}{\partial e^2_\varphi} \cdot \frac{\partial^2 f}{\partial e^2_\varphi}, \qquad R_{3,1}(a, f, \varphi) = \frac{\partial^3 a}{\partial e^3_\varphi} \cdot \frac{\partial f}{\partial e_\varphi}.$$

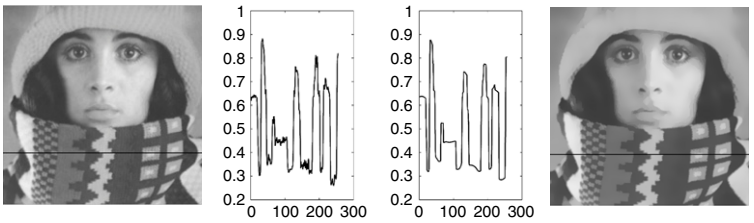

Fig. 5. Demonstrating the power of nonlinear diffusion for image filtering. Left: original image "trui". Right: after filtering with (26) and (27). Middle: a comparison of one-dimensional image slices of the original and filtered images.

Note that $R_{3,1}(a, f, \varphi) = R_{1,3}(f, a, \varphi)$ and $D_{1,3}(a, f) = D_{3,1}(f, a)$. Direct calculations show that

$$\int_0^{2\pi} R_{1,3}(a, f, \varphi)\, d\varphi = \frac{3\pi}{4} D_{1,3}(a, f) \quad \text{and} \quad \int_0^{2\pi} R_{2,2}(a, f, \varphi)\, d\varphi = \frac{3\pi}{4} D_{2,2}(a, f).$$

This completes our proof that the h^2-term in (25) is rotation invariant. □

Application to nonlinear diffusion image filtering. Accurate numerical implementations of nonlinear diffusion processes governed by

$$\frac{\partial u(x, y, t)}{\partial t} = \operatorname{div}\left(a(x, y, u, \nabla u)\nabla u\right), \qquad u(x, y, 0) = u_0(x, y), \tag{26}$$

subject to appropriate boundary conditions, are important for a number of disciplines including computational physics, magnetohydrodynamics, financial mathematics, and image processing. In particular, in image processing, adaptive image smoothing is often carried out by (26) with

$$a(x, y, u, \nabla u) = \exp(-|\nabla u|/\lambda), \tag{27}$$

as suggested by Perona and Malik in their seminal paper [33]. Fig. 5 demonstrates how our numerical implementation of (26) and (27) performs an adaptive image smoothing and removes texture from an image.

In image processing, the system (26), (27) is typically solved by finite differences methods with explicit or implicit Euler schemes and several dozens of iterations are usually required in order to achieve desired image filtering effects. For a number of applications including image segmentation and feature extraction, accurate estimation of the gradient directions in an image filtered by (26) and (27) is required. Unfortunately standard finite difference schemes have poor rotation-invariance properties. If such schemes are used repeatedly, the directional error is accumulated. See [34,10] for examples of finite difference schemes with improved rotation invariance properties.

Our approach to numerical solving of (26), (27) combines the explicit Euler scheme with obvious generalizations of the optimal rotation-invariant 3×3 stencils derived in previous sections for gradient, Laplacian, and quasi-Laplacian. To demonstrate advantages of our approach we apply our numerical implementation of (26), (27) to (23). Fig. 6 shows level sets of (23) before and after applying nonlinear diffusion (26), (27). We also compare our implementation with that from [35], where five-point stencils are used for numerical solving (26) and (27).

Frequency response analysis. Now we take a brief look at stencils (19) and (20) from a frequency point of view. This standpoint is important when dealing with phenomena possessing a range of space and time scales. Turbulent fluid flows, electromagnetic and acoustic wave propagation, multiresolution analysis of financial data, and multiscale image processing are among common examples.

For the sake of simplicity assume that our square grid has a unit step-size: $h = 1$ (this can be easily achieved by rescaling). One can see that (19) consists of the simplest central difference operator combined with a smoothing kernel applied to the orthogonal direction:

$$D_x = \frac{1}{2}\begin{bmatrix}-1 & 0 & 1\end{bmatrix} \cdot \frac{1}{w+2}\begin{bmatrix}1 & w & 1\end{bmatrix}^T. \tag{28}$$

The eigenvalue (also called the frequency response) of (19) corresponding to the eigenfunction $\exp(i(\omega_1 x + \omega_2 y))$ is given by

$$i \sin\omega_1 \cdot \frac{w+2}{w+2\cos\omega_2}, \quad -\pi < \omega_k < \pi,\ k = 1, 2,$$

where the first term of the product is the frequency response for the central difference and the second one corresponds to the smoothing kernel in (28).

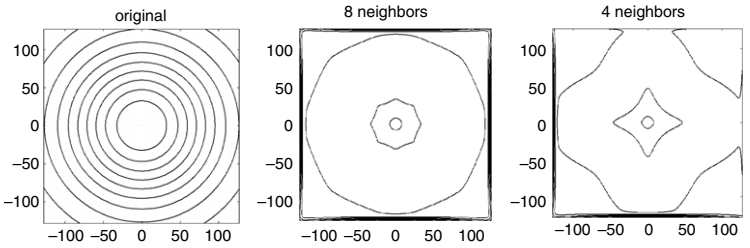

Fig. 6. Left: the contour lines of Gaussian bump function (23) are perfect circles. Middle: contours of the Gaussian filtered using our implementation of nonlinear diffusion (26), (27). Right: contours of the Gaussian filtered using code from [35].

It is well known that the frequency response $i \sin \omega$ delivers a satisfactory approximation of $i\,\omega$, the frequency response for the ideal derivative, only for sufficiently small frequencies ω (see, for example, [36, Section 6.4]). Now it is clear how (19) improves the central difference: smoothing due to the use the central difference operator instead of the true x-derivative is compensated by adding a certain amount of smoothing in the y-direction. Thus (19) and its y-direction counterpart do a better job in estimating the gradient direction than in estimating the gradient magnitude.

If the goal is to achieve an accurate estimation of both the gradient direction and magnitude, we can combine (19) and (20) as follows. Note that

$$1 + \frac{1}{w+2} L_\Delta = \frac{1}{(w+2)^2} \begin{bmatrix} 1 & w & 1 \\ w & w^2 & w \\ 1 & w & 1 \end{bmatrix} = \frac{1}{w+2} \begin{bmatrix} 1 & w & 1 \end{bmatrix} \cdot \frac{1}{w+2} \begin{bmatrix} 1 \\ w \\ 1 \end{bmatrix},$$

which can be considered as simultaneous smoothing (averaging) with respect to both the coordinate directions. Thus it is natural to use

$$\left(1 + \frac{1}{w+2} L_\Delta\right)^{-1} D_x \tag{29}$$

which combines (19) with a Laplacian-based sharpening. The frequency response function corresponding to (29) is given by

$$H(\omega) = i \sin \omega \cdot \frac{w+2}{w + 2\cos\omega}, \tag{30}$$

where parameter w should be chosen in such a way that (30) delivers a good approximation of $i\omega$, the frequency response for the true derivative. For example, the Taylor series expansion of (30) with respect to ω at $\omega = 0$ shows that the best approximation of the exact x-derivative for $\omega \ll 1$ is achieved when $w = 4$ which corresponds to a Padé approximation. However this choice of parameter w is not optimal if we deal with a wider range of frequencies.

Note that (29) is equivalent to an implicit finite difference scheme

$$\frac{1}{w+2} \left(f'_{i-1,j} + w f'_{i,j} + f'_{i+1,j}\right) = \frac{1}{2} \left(f_{i+1,j} - f_{i-1,j}\right). \tag{31}$$

Implicit finite differences are widely used for accurate numerical simulations of physical problems involving linear and nonlinear wave propagation phenomena, see, for example, [37], [38, Section 5.8]. An implicit finite difference scheme is usually characterized by its frequency-resolving efficiency, the range of frequencies ω over which a satisfactory approximation of the corresponding differential operator is achieved.

Motivated by [39,40] where a frequency-based analysis of simple 3×3 stencils for first-order derivatives was performed, we found out that (30), (31) with $w = 10/3$ deliver a good frequency resolving efficiency for a sufficiently large frequency range, as seen in Fig. 7. Of course, the problem of finding an optimal w is application-dependent and the optimal value of w depends on optimization criteria used and a range of frequencies where the optimization is sought.

The approach via Minkowski's theorem and Veronese map developed in Section 2 is suggestive for an extension of the above results to 3D and to grids in any dimensions. We leave this for future publication.

Acknowledgments

B.K. is grateful to the Ecole Polytechnique in Paris and the Max Planck Institute in Bonn for their hospitality during the completion of this paper. He was partially supported by an NSERC research grant. S.T. was partially supported by the Simons Foundation grant No 209361 and by the NSF grant DMS-1105442.

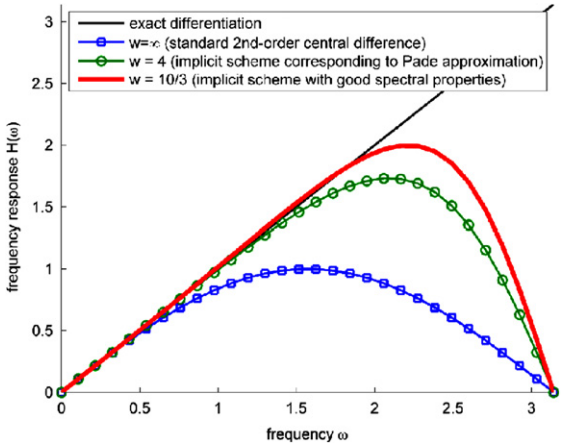

Fig. 7. Visual frequency-response analysis of (29) for various values of parameter w. Notice good frequency-resolving efficiency of (30) with $w = 10/3$.

References

[1] A. Friedman, W. Littman, Functions satisfying the mean value property, Transactions of the American Mathematical Society 102 (1) (1962) 167–180.
[2] A.H. Stroud, Approximate Calculation of Multiple Integrals, Prentice-Hall, 1971.
[3] F. Natterer, The Mathematics of Computerized Tomography, SIAM, 2001.
[4] R. Schneider, Convex Bodies: The Brunn–Minkowski Theory, Cambridge University Press, 1993.
[5] J. Harris, Algebraic Geometry: A First Course, Springer, 1992.
[6] V. Arnold, B. Khesin, Topological Methods in Hydrodynamics, Springer, 1998.
[7] S. Childress, Fast dynamo theory, in: Topological Aspects of the Dynamics of Fluids, Kluwer Academic Publishers, Dordrecht, 1992, pp. 111–147.
[8] J. Weickert, Anisotropic Diffusion in Image Processing, Teubner-Verlag, Stuttgart, 1998.
[9] G. Aubert, P. Kornprobst, Mathematical Problems in Image Processing, 2nd ed., Springer, 2006.
[10] J. Weickert, H. Scharr, A scheme for coherence-enhancing diffusion filtering with optimized rotation invariance, Journal of Visual Communication and Image Representation 13 (2002) 103–118.
[11] T. Langer, A. Belyaev, H.-P. Seidel, Exact and interpolatory quadratures for curvature tensor estimation, Computer Aided Geometric Design 24 (8–9) (2007) 443–463.
[12] G. Taubin, Estimating the tensor of curvature of a surface from a polyhedral approximation, in: Proc. ICCV'95, 1995, pp. 902–907.
[13] H. Pottmann, J. Wallner, Q. Huang, Y.-L. Yang, Integral invariants for robust geometry processing, Computer Aided Geometric Design 26 (2009) 37–60.
[14] Q. Mérigot, M. Ovsjanikov, L. Guibas, Robust Voronoi-based curvature and feature estimation, in: Proc. of SIAM/ACM Joint Conference on Geometric and Physical Modeling, 2009, pp. 1–12.
[15] J.J. Koenderink, A.J. Van Doorn, Surface shape and curvature scales, Image and Vision Computing 10 (1992) 557–565.
[16] J.R. Bradford, D.R. Westhead, Improved prediction of protein–protein binding sites using a support vector machines approach, Bioinformatics 21 (8) (2005) 1487–1494.
[17] L. Zhong, Y. Su, S.-Y. Yeo, R.-S. Tan, D.N. Ghista, G. Kassab, Left ventricular regional wall curvedness and wall stress in patients with ischemic dilated cardiomyopathy, American Journal of Physiology—Heart and Circulatory Physiology 296 (2009) H573–H584.
[18] R. Valenti, N. Sebe, T. Gevers, Image saliency by isocentric curvedness and color, in: IEEE International Conference on Computer Vision, 2009.
[19] P. Delsarte, J.M. Goethals, J.J. Seidel, Spherical codes and designs, Geometriae Dedicata 6 (1977) 363–388.
[20] Y. Hong, On spherical t-designs in r^2, European Journal of Combinatorics 3 (1982) 255–258.
[21] P.D. Seymour, T. Zaslavsky, Averaging sets: a generalization of mean values and spherical designs, Advances in Mathematics 52 (1984) 213–224.
[22] E. Bannai, E. Bannai, A survey on spherical designs and algebraic combinatorics on spheres, European Journal of Combinatorics 30 (6) (2009) 1392–1425.
[23] M. Patra, M. Karttunen, Stencils with isotropic discretisation error for differential operators, Numerical Methods for Partial Differential Equations 22 (4) (2005) 936–953.
[24] M. Wardetzky, S. Mathur, F. Kälberer, E. Grinspun, Discrete Laplace operators: no free lunch, in: Proceedings of Fifth Eurographics Symposium on Geometry Processing, Barcelona, Spain, July 2007, pp. 33–37.
[25] W. Gordon, J. Wixom, Pseudo-harmonic interpolation on convex domains, SIAM Journal on Numerical Analysis 11 (5) (1974) 909–933.
[26] A. Belyaev, On transfinite barycentric coordinates, in: Proceedings of Fourth Eurographics Symposium on Geometry Processing, Sardinia, Italy, July 2006, pp. 89–99.
[27] W.K. Pratt, Digital Image Processing, 3rd ed., John Wiley & Sons, 2001.
[28] R.C. Gonzalez, R.E. Woods, Digital Image Processing, 3rd ed., Pearson Prentice Hall, 2008.
[29] Behzad Kamgar-Parsi, Behrooz Kamgar-Parsi, Azriel Rosenfeld, Optimally isotropic Laplacian operator, IEEE Transactions on Image Processing 8 (10) (1999) 1467–1472.
[30] W.G. Bickley, Finite difference formulae for the square lattice, The Quarterly Journal of Mechanics and Applied Mathematics 1 (1948) 35–42.
[31] L.V. Kantorovich, V.I. Krylov, Approximate Methods of Higher Analysis, Noordhoff-Interscience, 1956.
[32] G. Birkhoff, R.E. Lynch, Numerical Solution of Elliptic Problems, SIAM, 1984.
[33] P. Perona, J. Malik, Scale-space and edge detection using anisotropic diffusion, IEEE Transactions on Pattern Analysis and Machine Intelligence 12 (7) (1990) 629–639.
[34] J. Weickert, Anisotropic diffusion filters for image processing based quality control, in: Proc. Seventh European Conf. on Mathematics in Industry, Teubner-Verlag, 1994, pp. 355–362.
[35] P. Perona, T. Shiota, J. Malik, Anisotropic Diffusion, Kluwer Academic Press, 1994, pp. 73–92.
[36] R.W. Hamming, Digital Filters, 3rd ed., Dover, 1998.
[37] T. Colonius, S.K. Lele, Computational aeroacoustics: progress on nonlinear problems of sound generation, Progress in Aerospace Science 40 (6) (2004) 345–416.
[38] T. Petrila, D. Trif, Basics of Fluid Mechanics and Introduction to Computational Fluid Dynamics, Springer, 2005.
[39] H. Scharr, S. Körkel, B. Jähne, Numerische isotropieoptimierung von fir-filtern mittels querglättung, in: Proc. DAGM'97, 1997, pp. 367–374.
[40] B. Jähne, H. Scharr, S. Körkel, Principles of filter design, in: Handbook of Computer Vision and Applications, in: Signal Processing and Applications, vol. 2, Academic Press, 1999, pp. 125–151.